Superoscillatory quartz lens with effective numerical aperture greater than one

G. H. Yuan[1*], Y.-H. Lin[2], D. P. Tsai[2,3], N. I. Zheludev[1,4]

[1]Centre for Disruptive Photonic Technologies, The Photonics Institute, SPMS, Nanyang Technological University, Singapore 637371, Singapore

[2]Taiwan Instrument Research Institute, NARLabs, Hsinchu, Taiwan

[3]Department of Electronic Information Engineering, The Hong Kong Polytechnic University, Hung Hom, Kowloon, Hong Kong

[4]Optoelectronics Research Centre & Centre for Photonic Metamaterials, University of Southampton, Southampton SO17 1BJ, UK

**Corresponding author: ghyuan@ntu.edu.sg*

Abstract

We report super-resolution high-numerical-aperture and long-working-distance superoscillatory quartz lenses for focusing and imaging applications. At the wavelength of λ=633 nm, the lenses have an effective numerical aperture of 1.25, working distance of 200 μm and focus into a hotspot of 0.4λ. Confocal imaging with resolution determined by the superoscillatory hotspot size is experimentally demonstrated.

High-numerical-aperture and long-working-distance planar optical lenses are highly desirable for applications in miniaturized mobile devices, camera lenses, super-resolved microscopes, and others. Considerable progress has been achieved in recent years in developing metasurface flat lenses that mimic conventional convex glass lenses with gradient arrays of tailored dielectric scatterers [1-3]. The resolution of such lenses is diffraction-limited: they cannot focus beyond $\frac{\lambda}{2\,NA}$ where λ is the wavelength of light and $NA = \frac{R}{\sqrt{R^2+f^2}}$ is the lens' numerical aperture (NA) which is always less than unity. Here R is the lens' radius and f is its focal distance.

However, focusing beyond the diffraction limit is possible using the phenomenon of super-oscillation when precisely tailored interference of propagating waves diffracted on a mask forms a small hot-spot in the optical far-field without any contributions from the evanescent waves [4,5]. Such masks are termed superoscillatory lenses (SOLs). In principle, SOLs can focus into a hotspot of any size, but this comes at a cost of only a diminishing fraction of light

energy going into the smaller hotspot: the rest of light energy forms a "halo" (sideband) of light surrounding the central hotspot. Binary transmission and phase retardation SOLs [6-8] and more sophisticated greyscale metasurfaces SOLs [9] have been developed with an effective numerical aperture for the central hotspot of up to NA=1.52. The superoscillatory focusing can be used in imaging [10] and this technology has been successfully used in confocal microscopes for biological [11,12] and nanotechnology imaging with sub-diffraction resolution [6-8, 13,14], in nanometrology [15] and optical trapping applications [16]. However, the radius R of previously reported SOLs was limited to a few tens of microns and focal distances to about less than 20 wavelengths, which limited their wider applications. The short working distance (typically 10 μm to 15 μm) prohibits the use of conventional coverslips and great care is required to safely position the lens at close proximity of objects without damaging either the lens or the object, and therefore imaging of complex volume structures is prohibited.

Here we report large SOLs with dimensions comparable with conventional commercial high-NA lenses. The SOLs with diameter $2R$ = 1.2 mm are fabricated in quartz by optical lithography that allows low-cost mass-production. At a wavelength of 633 nm, the SOLs with a working distance up to f = 200 μm focuses light into superoscillatory hotspots with full-width at half-maximum (FWHM) of 0.4λ. This corresponds to an effective NA = 1.25. A conventional singlet lens with such focal distance and diameter would have NA=0.95 and will focus into a hotspot of ~ 0.53λ.

No.	**1**	**2**	**3**	**4**	**5**	**6**	**7**	**8**	**9**	**10**	**11**	**12**	**13**	**14**	**15**
Radius (μm)	18.24	37.85	50.22	80.93	113.99	122.42	146.20	177.31	186.71	199.51	224.25	241.53	252.75	277.83	297.39
Width (μm)	5.64	6.20	8.16	5.30	3.88	5.93	32.42	7.26	4.72	5.00	17.39	3.11	9.48	8.30	4.27
No.	**16**	**17**	**18**	**19**	**20**	**21**	**22**	**23**	**24**	**25**	**26**	**27**	**28**	**29**	**30**
Radius (μm)	311.89	343.36	355.77	371.37	386.34	394.83	417.89	433.99	458.78	492.71	504.86	529.87	546.19	564.98	587.10
Width (μm)	5.56	12.07	4.50	5.42	3.68	7.01	4.90	13.19	15.29	6.14	6.02	22.53	3.30	18.13	19.44

Table 1. Design parameters of the binary phase SOL mask which has 30 etched rings with varying radius and width producing a 180° phase retardation.

The SOLs reported here are binary phase masks, a concentric set of rings etched into a 1mm thick quartz substrate. The required depth of etching depends on the targeted operation wavelength. It is selected such that the light passing through the ring gains an additional phase shift of 180° with respect to the light directly passing through the substrate. The SOL is designed as a set of 30 rings with the multi-objective particle swarm optimization algorithm

that optimizes the targeted hotspot using two circular prolate spheroidal wavefunctions decomposition [9] and vectorial diffraction theory [17], see Table 1.

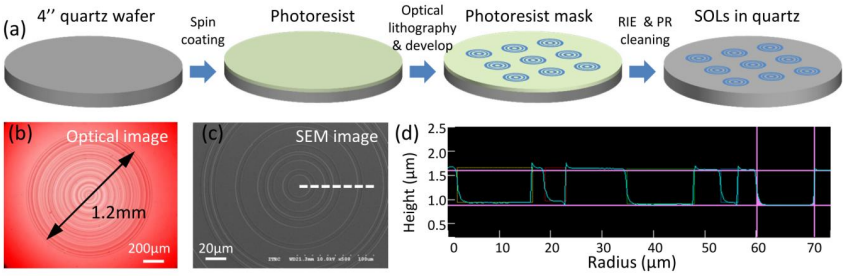

Figure 1. (**a**) Fabrication procedures of the quartz superoscillatory lens (SOL) including spin coating, lithography and development of photoresist, reactive ion etching and photoresist cleaning. (**b**) Optical image of an SOL with a diameter of 2*R*=1.2 mm. (**c**) SEM image of the central part of the SOL. (**d**) Profile of the lens measured along the white dashed line in (c) shows etching depth of 710 nm ± 18 nm corresponding to a phase delay of (1.1±0.03)π at the wavelength of 633 nm.

The fabrication procedures of the quartz SOLs is shown in Fig. 1(a), while Figs. 1(b), 1(c) and 1(d) show the detailed optical and SEM image of the SOL and its height profile respectively. The prevailing nanofabrication techniques including electron beam lithography and focused ion beam milling are not suitable for mass production. Instead we used the CMOS compatible optical lithography on highly transparent quartz wafer that is suitable for in-parallel fabrication of multiple optical components on a single-crystal. The simulated field intensity profiles of the SOL in the propagation cross-section (*yz* plane near the designed focus) and transverse plane at the focus (*xy* plane, z = 200 µm) are shown in Figs. 2(a) and 2(b) respectively. The FWHM of the superoscillatory focus is 0.4λ, corresponding to an effective NA=1.25. The ratio of intensities in the first sideband and the central hotspot is 45.2%.

Performance of such lenses was characterized experimentally and tested in imaging experiments. Since the superoscillatory field is formed by interference of free-space propagating waves, its intensity profile can be directly mapped by the optical microscope with no loss of resolution [6]. For experimental characterization, we used a high-NA objective (Nikon CFI LU Plan APO EPI 150X, NA=0.95). The overall magnification of the microscope equipped with an sCMOS camera with a pixel size of 6.5µm was 500X. The experimentally measured intensity profiles are in good agreement with theoretical predictions, see Figs. 2(c) and 2(d): the attainable spot size of 0.41λ at z = 200 µm is slightly larger than the simulation

value of 0.4λ due to fabrication and incident wavefront imperfections. The axial intensity profiles and spot sizes show good agreement between the simulation and experiment as seen from Fig. 2(e) and Fig. 2(f). We also evaluated the Strehl ratio defined as the intensity ratio between the designed superoscillaory hotspot and Airy disk at the same total power of incident light. The throughput to focus efficiency of the SOL is somewhat lower than that of comventional diffraction-limited lens: the expected (simulated) and actual (measured) Strehl ratios are 0.266 and 0.126 respectively (the actual value is lower due to fabrication inperfection) , approaching the upper limit of the Strehl ratio at a given hotspot size [18].

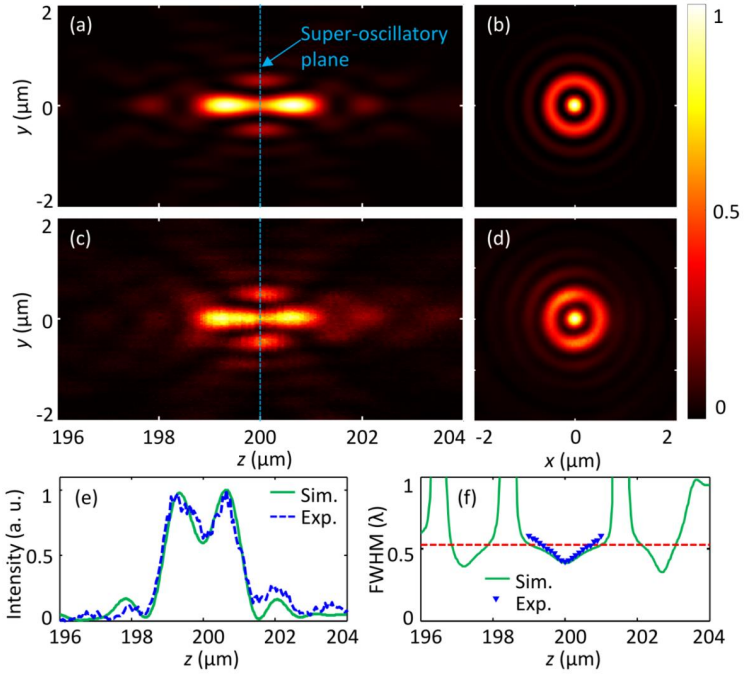

Figure 2. (**a**) Simulated longitudinal cross-section of the superoscillatory hotspot near an axial distance of 200μm. (**b**) Simulated intensity profile in the transverse plane. (**c**) Experimentally measured longitudinal cross-section of the superoscillatory hotspot in the same area of interest. (**d**) Experimental intensity profile in the transverse plane. (**e**) Comparison of axial intensity of the hotspot between simulation (green curve) and experiment (blue dashed curve). (**f**) Comparison of spot size between simulation (green curve) and experiment (blue down triangle). The red dashed line shows the Abbe diffraction limit defined by λ/(2NA)=0.53λ.

To demonstrate the imaging capabilities of the quartz SOL, we used a confocal arrangement with circularly polarized illumination at λ=633 nm, a 100X objective lens and a pinhole aperture at the detector plane, as shown in Fig. 3(a). Circularly polarized light is used

to generate a more rotationally symmetric hotspot and mitigate the depolarization effect. We first tested the limit of resolution of the quartz SOL and compared with a conventional diffraction-limited objective (NA=0.95). The first set of test objects were pairs of nanoholes (diameter of 160 nm) with varying distance from 210 nm to 390 nm with a step of 30 nm fabricated by focused ion beam milling in a 100 nm-thickness gold film on a glass slip, see Fig. 3(b). With the SOL a hole center-to-center distance of 240 nm can be nearly resolved according to the Abbe criterion, where the valley to peak ratio is around 0.974. For distance from 270 nm, 300 nm, 330 nm, 360 nm to 390 nm, the valley to peak ratio decreases from 0.876, 0.788, 0.734, 0.584 to 0.495 respectively. In comparison, a conventional diffraction-limited objective (NA=0.95) can only resolve holes spaced by a distance of 330 nm (valley to peak ratio of 0.969) and above using the same criterion. A considerable image resolution improvement can also be seen with more complex objects comprising of nanohole arrays arranged in 'Ursa Major' and 'Ursa Minor' constellations layout, as shown in Fig. 3(c): the smallest hole-to-hole distance of 264 nm (0.42λ) can be resolved by the SOL but cannot be distinguished by diffraction-limited objective.

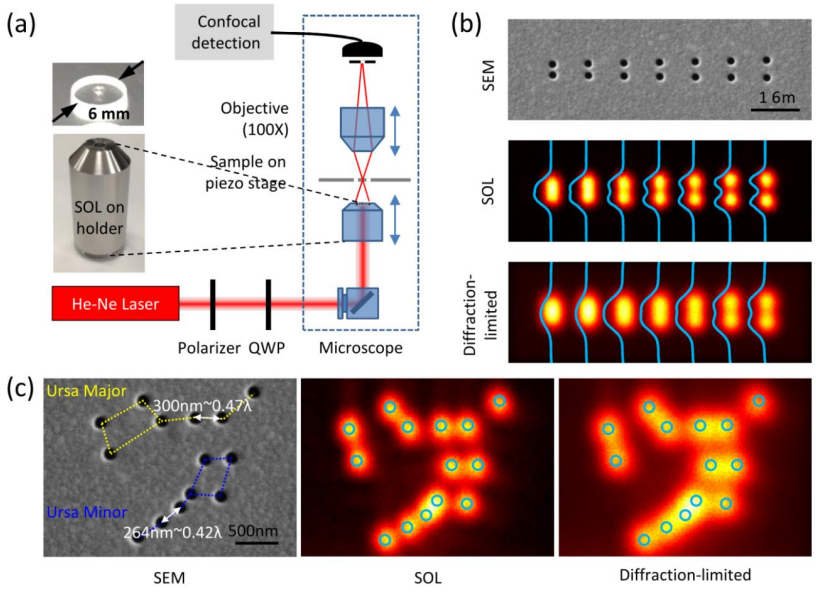

Figure 3. (**a**) Schematics of the experimental setup for the imaging with superoscillatory hotspot and confocal detection. Insets show the 1.2 mm-diameter SOL in the laser diced quartz substrate with 6 mm diameter (top) and the self-manufactured holder with an open aperture to fit the SOL (bottom). (**b**) SEM image, superoscillatory (with SOL) and diffraction-limited (with a normal objective of NA=0.95) imaging of hole pair arrays with varying center-to-center distance from 210 nm to 390 nm with a step size of 30 nm. Hole diameter: 160 nm. (**c**)

SEM image, superoscillatory and diffraction-limited imaging of a complex image (Ursa Major in yellow, Ursa Minor in blue) with varying hole center-to-center distance. Hole diameter: 160 nm.

In summary, we report quartz superoscillatory lenses fabricated in a CMOS compatible high-throughput optical lithography process. The lenses, with only 1 mm thickness and having effective NA=1.25 and focal distance of 316λ, were fabricated. Designed for the wavelength of 633 nm, they focus light into the hotspot of 253 nm (~0.4λ). Such compact and powerful lenses can find applications in confocal imaging and metrology instruments.

This work was supported by the Singapore Ministry of Education (Grant No. MOE2016-T3-1-006), the Agency for Science, Technology and Research (A*STAR) Singapore (Grant No. SERC A1685b0005), the Engineering and Physical Sciences Research Council UK (Grants No. EP/N00762X/1 and No. EP/M009122/1). The data from this paper can be obtained from the University of Southampton ePrints research repository (https://doi.org/10.5258/SOTON/D1381).

References:

1. S. Wang, P. C. Wu, V.-C. Su, Y.-C. Lai, M.-K. Chen, H. Y. Kuo, B. H. Chen, Y. H. Chen, T.-T. Huang, J.-H. Wang, R.-M. Lin, C.-H. Kuan, T. Li, Z. Wang, S. Zhu, and D. P. Tsai, "A broadband achromatic metalens in the visible," Nat. Nanotech. **13**, 227 (2018).
2. W. T. Chen, A. Y. Zhu, V. Sanjeev, M. Khorasaninejad, Z. Shi, E. Lee, and F. Capasso, "A broadband achromatic metalens for focusing and imaging in the visible," Nat. Nanotech. **13**, 220 (2018).
3. M. Khorasaninejad, W. T. Chen, R. C. Devlin, J. Oh, A. Y. Zhu, and F. Capasso, "Metalenses at visible wavelengths: Diffraction-limited focusing and subwavelength resolution imaging," Science **352**, 1190 (2016).
4. M. V. Berry, and S. Popescu, "Evolution of quantum superoscillations and optical superresolution without evanescent waves," J. Phys. A: Math. Gen. **39**, 6965 (2006).
5. F. M. Huang, and N. I. Zheludev, "Super-resolution without evanescent waves," Nano Lett. **9**, 1249 (2009).
6. E. T. F. Rogers and N. I. Zheludev, "Optical superoscillations: Sub-wavelength light focusing and super-resolution imaging," J. Opt. **15**, 094008 (2013).

7. K. Huang, F. Qin, H. Liu, H. Ye, C.-W. Qiu, M. Hong, B. Luk'yanchuk, and J. Teng, "Planar diffractive lenses: fundamentals, functionalities, and applications," Adv. Mater. **30**, 1704556 (2018).
8. G. Chen, Z.-Q. Wen, and C.-W. Qiu, "Superoscillation: from physics to optical applications," Light Sci. Appl. **8**, 56 (2019).
9. G. H. Yuan, K. S. Rogers, E. T. F. Rogers, and N. I. Zheludev, "Far-field superoscillatory metamaterials superlens," Phys. Rev. Appl. **11**, 064016 (2019).
10. F. M. Huang, T. S. Kao, V. A. Fedotov, Y. Chen, and N. I. Zheludev, "Nanohole array as a lens," Nano Lett. **8**, 2469 (2008).
11. E. T. Rogers, S. Quraishe, J. L. Bailey, T. A. Newman, J. E. Chad, N. I. Zheludev, P. J. Smith, "Super-oscillatory imaging of nanoparticle interactions with neurons," Biophys. J. **108**, 479a (2015).
12. E. T. F. Rogers, S. Quraishe, K. S. Rogers, T. A. Newman, P. J. S. Smith, and N. I. Zheludev, "Far-field unlabelled super-resolution imaging with superoscillatory illumination," APL Photonics, in press (2020).
13. A. M. H. Wong, and G. V. Eleftheriades, "An optical super-microscope for far-field, real-time imaging beyond the diffraction limit," Sci. Rep. **3**, 1715 (2013).
14. F. Qin, K. Huang, J. F. Wu, J. H. Teng, C. W. Qiu, and M. H. Hong, "A supercritical lens optical label-free microscopy: sub-diffraction resolution and ultra-long working distance," Adv. Mater. **29**, 1602721 (2017).
15. G. H. Yuan, and N. I. Zheludev, "Detecting nanometric displacements with optical ruler metrology," Science **364**, 771 (2019).
16. B. K. Singh, H. Nagar, Y. Roichman, and A. Arie, "Particle manipulation beyond the diffraction limit using structured super-oscillating light beams," Light Sci. Appl. **6**, e17050 (2017).
17. G. H. Yuan, E. T. F. Rogers, T. Roy, G. Adamo, Z. X. Shen, and N. I. Zheludev, "Planar super-oscillatory lens for sub-diffraction optical needles at violet wavelengths," Sci. Rep. **4**, 6333 (2014).
18. H. Shim, H. Chung, and D. D. Miller, "Maximal free-space concentration of electromagnetic waves," arXiv: 1905.10500 (2019).